HHS Public Access

Author manuscript

*Neuroimage*. Author manuscript; available in PMC 2022 August 15.

Published in final edited form as:

*Neuroimage*. 2022 August 15; 257: 119292. doi:10.1016/j.neuroimage.2022.119292.

# Phenotypic and genetic associations between gray matter covariation and tool use skill in chimpanzees (*Pan troglodytes*): Repeatability in two genetically isolated populations

**M.M. Mulholland**[a,*], **S.J. Schapiro**[a,b], **C.C. Sherwood**[c], **W.D. Hopkins**[a]

[a] Department of Comparative Medicine, The University of Texas MD Anderson Cancer Center, 650 Cool Water Drive, Bastrop, TX 78602, USA

[b] Department of Experimental Medicine, University of Copenhagen, Copenhagen, Denmark

[c] Department of Anthropology and Center for the Advanced Study of Human Paleobiology, The George Washington University, Washington, DC 20052, USA

## Abstract

Humans and chimpanzees both exhibit a diverse set of tool use skills which suggests selection for tool manufacture and use occurred in the common ancestors of the two species. Our group has previously reported phenotypic and genetic associations between tool use skill and gray matter covariation, as quantified by source-based morphometry (SBM), in chimpanzees. As a follow up study, here we evaluated repeatability in heritability in SBM components and their phenotypic association with tool use skill in two genetically independent chimpanzee cohorts. Within the two independent cohorts of chimpanzees, we identified 8 and 16 SBM components, respectively. Significant heritability was evident for multiple SBM components within both cohorts. Further, phenotypic associations between tool use performance and the SBM components were largely consistent between the two cohorts; the most consistent finding being an association between tool use performance and an SBM component including the posterior superior temporal sulcus (STS) and superior temporal gyrus (STG), and the interior and superior parietal regions ($p < 0.05$). These findings indicate that the STS, STG, and parietal cortices are phenotypically and genetically implicated in chimpanzee tool use abilities.

### Keywords

Chimpanzee; Source-based morphometry; Tool use; Heritability



* Corresponding author. mmmulholland@mdanderson.org (M.M. Mulholland).

Credit authorship contribution statement

**M.M. Mulholland:** Formal analysis, Investigation, Data curation, Writing – original draft, Visualization. **S.J. Schapiro:** Investigation, Resources, Writing – review & editing, Project administration. **C.C. Sherwood:** Conceptualization, Data curation, Writing – review & editing, Funding acquisition. **W.D. Hopkins:** Conceptualization, Methodology, Formal analysis, Investigation, Data curation, Writing – original draft, Visualization, Supervision, Funding acquisition, Project administration.

Supplementary materials

Supplementary material associated with this article can be found, in the online version, at doi:10.1016/j.neuroimage.2022.119292.

## 1. Introduction

Besides having an unusually large brain, humans have evolved modifications to the anatomy of specific brain regions and networks of connectivity that reflect our unique technological and cognitive specializations. Specifically, a number of brain regions within the frontal and parietal cortex, have been implicated in the planning and execution of complex praxic functions, particularly as it relates to the manufacture and use of tools (Johnson-Frey, 2004; Lewis, 2006; Vaesen, 2012). Though humans exhibit a wide range of complex tool making and use skills, the capacity to manufacture and use tools is a shared behavioral trait between humans and a number of other species (Boysen et al., 1999; Candland, 1987; Fragaszy et al., 2004; Mendes et al., 2007; Moura and Lee, 2004; Phillips, 1998; Shumaker et al., 2011; Van Schaik et al., 2003; Visalberghi, 1990). For instance, among nonhuman primates, chimpanzees exhibit an assorted set of tool use skills in nature that reflect behavioral adaptations to ecological variation in available food resources. As a consequence, there is a diverse set of different types of tool use observed within and between different groups or communities of chimpanzees, such as termite fishing, ant dipping, algae dipping, nut cracking, wade dipping, pestle pounding, use of spears, and others (Boesch and Boesch, 1990; Boesch et al., 2017; Pruetz and Bertolani, 2007; Sanz and Morgan, 2007; Whiten et al., 2001; Whiten et al., 1999). These observations suggest there was strong selection for increasing tool manufacture and use skills in the common ancestor of humans and chimpanzees prior to their divergence ~ 6 million years ago which may have coincided with region specific changes in brain structure and organization, such as lateralization in structure and function (Bradshaw and Rogers, 1993; Gibson and Ingold, 1993; Van Schaik et al., 1999).

Though tool use is well documented in chimpanzees and other primate species, the genetic and neural foundation of tool use in nonhumans remains a topic of significant theoretical and empirical interest (Hecht et al., 2013; Peeters et al., 2009). Of specific interest to this study is the recent report by Hopkins et al. (2019) who examined gray matter covariation in chimpanzee brains using source-based morphometry (SBM). As described in Mulholland et al. (2020), SBM is a multivariate approach that utilizes information about relationships among voxels and then groups those carrying similar information across the brain. The resulting components represent similar covariation networks between subjects. The SBM produces a weighted score at the individual level that reflects each subject's relative contribution to the creation of each spatial component. Hopkins et al. (2019) identified 24 gray matter components in a sample of 226 chimpanzees, and further found that (1) there was significant heritability for 18 of the 24 SBM components, and (2) measures of tool use skill in the chimpanzees were both phenotypically and genetically associated with two of the components, suggesting a shared neuroanatomical and genetic mechanism underlying their expression. However, as noted by Hopkins et al. (2019), one limitation in the study was that, within the chimpanzee sample, there were two cohorts of apes that (1) differed in sample size (77 versus 139 subjects) and (2) were scanned on magnets with different field strengths (1.5 Tesla versus 3 Tesla). Scanner magnet strength, as well as the types of post image processing of the scans, can influence segmentation of gray and white matter, which may influence the identification of brain regions that contribute to the creation of

each component, as well as create potential artifacts in some components (i.e., were found on brain edges, or overlapped into regions not containing gray matter; see components 20, 22–24 in Hopkins et al. 2019 for examples). Since the 2015 NIH moratorium on biomedical research in chimpanzees, no new MRI data have been collected from the chimpanzees. However, we can utilize this important archival resource to test new hypotheses or address limitations of previous research.

The aims of the current study were two-fold and designed to address some of the previous limitations of the Hopkins et al. (2019) report. First, studies have shown that the inclusion and order of various preprocessing methods, such as brain extraction, bias correction, and denoising, can affect subsequent brain segmentation and analyses. For example, in studies of humans, brain extraction and bias correction resulted in more accurate warping of native space scans to template brains during voxel-based morphometry (Acosta-Cabronero et al., 2008). In addition, segmentation of gray and white matter was more accurate after a non-local means filter removed Rician noise (Eskildsen et al., 2011). For these reasons, we updated the preprocessing methods employed with the chimpanzee sMRI scans and provided details on these new post-image processing methods. Then we reexamined and described gray matter covariation in the chimpanzee brain using SBM and reported the heritability for each gray matter component within the entire sample. In addition, we tested for phenotypic correlations between tool use performance and the SBM components identified in the analysis after controlling for sex, age and scanner magnet.

Second, we evaluated the repeatability of the phenotypic association between tool use skill and the SBM gray matter components. Repeatability in findings in the behavioral, brain, and genomic sciences has become a topic of increasing interest (Baker, 2016a, 2016b; Lazic, 2010; McArthur, 2019) and here we took advantage of two population of apes to address this important issue. Specifically, as noted above, there were two distinct populations of chimpanzees in the Hopkins et al. (2019) report that (1) differed in sample size (77 versus 139 subjects) and (2) were scanned on magnets with different field strengths (1.5 Tesla versus 3 Tesla). Importantly, these two cohorts were also genetically isolated from each other. That is to say, the creation of these two cohorts of captive chimpanzees breeding populations were derived from different founder animals with no interbreeding taking place between the facilities that managed these apes. Thus, the two chimpanzee cohorts are genetically isolated from each other and, as we have argued before (Hopkins, Mareno and Schapiro, 2019; Hopkins et al., 2022), this offered a unique opportunity to evaluate repeatability in the phenotypic association between tool use skill and brain regions identified in the SBM components computed from within each cohort. To evaluate repeatability, separate SBM analyses were performed on the two chimpanzee cohorts. Because both the scanner magnet and the sample sizes differed between the two chimpanzee cohorts, we fully expected to find differences in the number of SBM components within each cohort. However, of specific interest was whether tool use performance measures were significantly associated with the weighted SBM scores derived for the SBM components within each cohort and, critically, if there was any overlap in the SBM components that were phenotypically associated with tool use skill between the two cohorts. Evidence of associations between tool use skill and brain regions that were common between SBM

components from the two cohorts would be evidence of independent replication in brain-behavior associations.

## 2. Materials and methods

### 2.1. Subjects

The subjects included 216 captive chimpanzees (132 females and 84 males) from the National Center for Chimpanzee Care (NCCC) at The University of Texas MD Anderson Cancer Center ($n$ = 139) or the Yerkes National Primate Research Center (YNPRC; $n$ = 77). All subjects were housed in indoor/outdoor enclosures, with 24 h access to both areas, except during cleaning. All enclosures included climbing structures, bedding, and daily environmental enrichment. Carestaff fed the chimpanzees a diet of commercial primate chow and fresh produce twice per day and provided them with several daily foraging opportunities and ad libitum access to water. All procedures performed with the chimpanzees were approved by the local Institutional Animal Care and Use Committees and followed all recommendations by the Institute of Medicine and NIH policy for the ethical treatment of chimpanzees in research.

### 2.2. Image acquisition

The *in vivo* magnetic resonance imaging (MRI) scans were previously obtained between 1996 and 2015 (ages 8–53; $M$ = 26.90 SD = 10.66), and collection of the scans was coordinated with the chimpanzees' annual physical examination to minimize the number of anesthesia events experienced by the apes. All MRI scans were acquired following YNPRC and NCCC standard procedures designed to minimize stress [as previously reported in Hopkins and Avants (2013), Hopkins et al. (2019), Mulholland et al. (2020)]. The animals were initially sedated with ketamine (10 mg/kg) or telazol (3–5 mg/kg), and then subsequently anaesthetized with propofol (40–60 mg/(kg/h)). Next, we transported each subject to the MRI scanning facility and placed them in a supine position in the scanner with their head in a human-head coil. Upon completion of the MRI, we singly housed each chimpanzee briefly (2–24 h), to permit close monitoring and safe recovery from the anesthesia, prior to returning them to their social group. The MRI data that support the findings of this study are available from the National Chimpanzee Brain Resource at https://www.chimpanzeebrain.org.

Seventy-seven chimpanzees (all from YNPRC) were scanned using a 3.0 Tesla scanner (Siemens Trio, Siemens Medical Solutions USA, Inc., Malvern, Pennsylvania, USA). T1-weighted images were collected using a three-dimensional gradient echo sequence (pulse repetition = 2300 ms, echo time = 4.4 ms, number of signals averaged = 3, matrix size = 320 × 320, with 0.6 × 0.6 × 0.6 resolution). The remaining 139 chimpanzees (from NCCC) were scanned using a 1.5T G.E. echo-speed Horizon LX MR scanner (GE Medical Systems, Milwaukee, Wisconsin, USA). T1-weighted images were collected in the transverse plane using a gradient echo protocol (pulse repetition = 19.0 ms, echo time = 8.5 ms, number of signals averaged = 8, matrix size = 256 × 256, with 0.7 × 0.7 × 1.2 resolution).

### 2.3. Post-image processing

Following acquisition, we processed all MRI data using an Apple iMac computer. The procedures, detailed below, were completed twice: once for the images acquired from the 1.5T scanner and again for those acquired from the 3.0T scanner. For each set of scans, following acquisition, we imported the raw DICOM files into 3D Slicer 4 (www.3Dslicer.org) and converted each into NifTI format (Fedorov et al., 2012; Kikinis et al., 2014) for use with the various programs used during post-image processing. See Table 1 for a summary of the updated preprocessing methods.

**2.3.1. Skull stripping—**First, we extracted the brain from the NifTI images using the Brain Extraction Tool (BET) function in the FMRIB Software Library (FSL; Oxford, UK). To ensure the entire skull was removed from the image without removing any portion of the brain, the fractional intensity thresholds for each subject ranged between 0.35 and 0.80 (Jenkinson et al., 2005; Smith, 2002). The resulting brain-extracted images for each subject were saved as a compressed NiFTI file.

**2.3.2. Bias correction—**The skull stripped NifTI images were subsequently imported into 3D Slicer for N4ITK bias correction (Boyes et al., 2008; Tustison et al., 2010; Tustison and Gee, 2009; Tustison et al., 2010, 2014). This automated process uses a variation of the nonparametric non-uniform normalization approach to correct for illumination non-uniformity in the image data, which can confound image analyses (Tustison et al., 2010). We used a spline distance of 50, a bias field of 0.15, and convergent threshold of 0.001 for all images. As before, the resulting bias-corrected images for each subject were saved as NiFTI files.

**2.3.3. Denoising—**Following bias correction, we denoised each image to improve image quality and performance of subsequent analyses. We used the MRI Denoising Package for MATLAB (R2015b; Mathworks, Natick, Massachusetts, USA) to denoise each scan using an optimized nonlocal means denoising filter (ONLM, Coupé et al. 2008). This program estimates the noise in the MRI data using the noise from the background. The resulting NiFTI files were saved for further processing.

**2.3.4. Resampling and alignment—**Following denoising, the scans were resampled at 0.625 mm isotropic voxels when imported into ANALYZE 11.0 (AnalyzeDirect, Overland Park, Kansas, USA). Then we manually aligned each scan on the Anterior Commissure-Posterior Commissure (AC-PC) axis and saved each in radiological space. To do so, we used a capsule placed during the imaging process as a directional marker for the left and right hemisphere. Finally, we used FSL to perform a 12-parameter affine linear registration (FLIRT, Jenkinson et al., 2002; Jenkinson and Smith, 2001) of the AC-PC aligned scan to a chimpanzee template brain (Hopkins and Avants, 2013).

**2.3.5. FSL-VBM pipeline—**Next, we ran each AC-PC aligned and affine registered brain scan through the FSL-VBM pipeline (http://fsl.fmrib.ox.ac.uk/fsl/fslwiki/FSLVBM). This process included (1) segmentation of each scan into gray and white matter, (2) linear registration of each scan to a standard chimpanzee template (Hopkins and Avants, 2013),

(3) creation of a study-specific gray matter template (Andersson et al., 2007; Douaud et al., 2007; Smith et al., 2004), (4) non-linear registration of each subject's gray matter image to the study-specific template, (5) modulation of the gray matter volume by use of a Jacobian warp to correct for local expansion or contraction of gray matter within each voxel, and (6) smoothing with an isotropic Gaussian kernel with a sigma of 2 mm.

**2.3.6. Linear registration—**Finally, each resulting image was reregistered to the chimpanzee template brain (Hopkins and Avants, 2013) using a 6-parameter rigid body linear registration in FSL (FLIRT, Hopkins and Avants, 2013; Jenkinson et al., 2002; Jenkinson and Smith, 2001), ensuring that the 1.5T and 3T scans had the same orientation and voxel dimensions. We used these scans in the subsequent source-based morphometry analysis.

## 2.4. Tool use performance assessment

Tool use performance was quantified in 202 chimpanzees in 2015 using a device that was designed to simulate termite fishing in wild chimpanzees. Details of the testing method have been described in detail elsewhere (Hopkins et al., 2019, 2015). Briefly, a PVC pipe was attached to the subject's home cage that was blocked at one end and had a small opening on the opposite end. Food with an adhesive quality was placed inside the PVC pipe and in order to obtain the food, the chimpanzee had to insert a small lollipop stick into the hole, then extract the stick and consume the food that adhered to the stick. The latency to successfully insert the stick was recorded on 50 responses for each chimpanzee (measured from the time the subject initiated an attempt to insert the tool with one hand and ended when the chimpanzee successfully inserted and removed the tool; Hopkins et al. 2019, 2015). The average latency of the 50 responses served as the outcome measure of interest. Because the two chimpanzee cohorts had different experiences with this tool use device, within the NCCC and YNPRC cohorts, the average latency scores were converted to standardized *z*-scores and we removed five chimpanzees from all subsequent analyses that were identified as outliers within each cohort (those with *z*-scores > 3.0). This included three individuals within the NCCC and two in the YNPRC cohort, thereby reducing the sample to 195 chimpanzees for all further analyses. The remaining 197 chimpanzees were between 5–50 years of age (Mean = 24.80, SD = 10.39) when tool use data performance was collected. The majority of the tool use data were obtained within 2 to 4 years of the acquisition of their MRI scans.

## 2.5. Statistical analyses: source-based morphometry

We ran three source-based morphometry analyses using the Group ICA of fMRI Toolbox (GIFT; http://icatb.sourceforge.net) in MATLAB R2015b. See Xu et al. (2009) and Gupta et al. (2019) for detailed descriptions of the computational methods used to develop the SBM analysis and its applications. For the first SBM (reported previously in Hopkins et al., 2020), we imported the smoothed, registered gray matter volumes for each subject ($N = 216$) and allowed the software to estimate the number of components based on the independent component analysis using a neural network algorithm. After estimation, the program calculates the parameters and creates a 4D volume containing each of the independent components. At the individual level, SBM produces a weighted score that

reflects each subject's relative contribution to the creation of each spatial component. To examine the brain regions contributing to each component, we registered the component maps (scaled to standard deviation units and z-scores) to the standard chimpanzee template brain and set the z-score threshold at $|z| \geq 3.00$ as has been used in previous studies in humans and chimpanzees (see Hara et al. 2012, Hopkins et al. 2019, Rogers et al. 2010, Xu et al. 2009). All voxels reaching this threshold were considered significant. The volume of each resulting brain region was then measured using the region-of-interest tool in ANALYZE 11.0. We then repeated the SBM analysis described above separately for each colony (NCCC $n = 139$; YNPRC $n = 77$). We then visually inspected the resulting colony specific SBM components for overlap in brain regions. If any components appeared to overlap between the two colonies, we performed a conjunction analysis. To determine the degree of similarity, we binarized and thresholded the component from each colony > 3.0, then added the binary volumes together to determine the regions that were overlapping between these two components.

### 2.6. Heritability, and phenotypic and genetic association between tool use skill and SBM components

We used the SOLAR (Sequential Oligogenic Linkage Analysis Routines) software package in two different ways. First, to estimate the heritability of brain components identified in the SBM analysis. Second, to assess genetic associations between tool use skill and SBM components. SOLAR takes into account the entire chimpanzee pedigree for these analyses; specifically, the identification codes of offspring, dam/mother and sire/father (when known) dating as far back as possible into the inception of each chimpanzee colony were entered into a file as well as their sex and rearing history. These data were then imported into SOLAR to create the pedigree structure. The pedigree structure of the entire chimpanzee sample has been published elsewhere (Hopkins et al., 2015) with some animals being fourth generation related to each other.

Prior to testing heritability, the phenotype values were normalized (due to high kurtosis) using an inverse normal transformation function within SOLAR. Covariates included age, sex, and scanner magnet. We used a polygenic model that estimated the influence of additive genetic variation (based on the pedigree) and the covariates, calculated heritability and its associated p-value, as well as the proportion of variance accounted for by the final covariates included in the model (see Almasy and Blangero 1998 for details about the theoretical background and calculations behind SOLAR). The significance level for the heritability of each SBM component was set at $p \leq 0.05$. As we have previously reported, tool use skill is significantly heritable in chimpanzees (Hopkins et al., 2019; Hopkins et al., 2015) and is phenotypically and genetically associated with variation in gray matter variation in the STS (Hopkins et al., 2019). To evaluate whether these results would replicate using the new preprocessing steps, we initially calculated partial correlation coefficients between the tool use skill measure and the weighted scores for each of the 19 combined sample SBM components, while statistically controlling for relatedness, scanner, sex, and age. SOLAR was then used to test for genetic associations between tool use skill and the related SBM components identified above. We also tested for phenotypic associations between tool use skill and the separate SBM components derived for the NCCC and YNPRC cohorts. As

before, we performed partial correlation coefficients between the tool use skill measure and the weighted scores for each SBM component within the NCCC and YNPRC cohorts. Sex and age were statistically controlled for in these analyses.

## 3. Results

### 3.1. Combined sample: source-based morphometry

The SBM analysis identified 19 independent components (groups of gray matter voxels that are highly correlated with each other across subjects), and calculated an individual weighted score reflecting each subject's contribution to each component. Provided in Table 2 is a full anatomical description of each component and their respective volumes. The largest regions in each component are as follows: 1. Supramarginal gyrus, 2. middle and superior temporal cortex, 3. temporal pole, amygdala and fusiform, 4. cerebellar cortex, 5. superior parietal cortex, 6. precuneus and superior parietal cortex, 7. rostral middle frontal cortex, 8. superior parietal cortex and paracentral, 9. lingual cortex, pericalcarine, and cuneus, 10. medial orbital frontal cortex, rostral anterior cingulate and the accumbens area, 11. rostral and caudal middle frontal cortex, 12. cerebellar cortex, 13. lateral occipital cortex and inferior parietal, 14. anterior superior, middle, and inferior temporal cortices, 15. cerebellar cortex, 16. cerebellar cortex, 17. precuneus, inferior parietal and lateral occipital cortex, 18. accumbens area, caudate, putamen, and pallidum, and 19. superior frontal cortex and anterior cingulate cortex. Supplementary materials include 3D renderings displaying the positive and negatively weighted regions of each component.

### 3.2. Combined sample: heritability

We used quantitative genetic methods to determine the degree of heritability in the weighted scores for the components identified in the SBM analysis. We found that 15 of the 19 SBM components were significantly heritable at the $p \leq 0.05$ level. The covariates (sex, age at MRI, and scanner magnet) explained, on average, 30% of the variability in weighted SBM component scores. The heritability ($h^2$) ranged from 0.18 to 0.87, with the highest heritability revealed for component 1 ($h^2 = 0.87$, $p \leq 0.001$), followed by component 2 ($h^2 = 0.62$, $p \leq 0.001$), and the lowest heritability revealed for component 12 ($h^2 = 0.18$, $p = 0.10$) (see Table 3 and Fig. 1a). Significant covariate effects of scanner magnet were found for 16 of the 19 components, which was not surprising as the scanner magnet influences gray and white matter contrast. Age accounted for a significant proportion of variance in 12 components, while sex accounted for a significant proportion of variance in 7 components. Table 3 shows the heritability estimates and contributions of each covariate for each of the 19 SBM components. Shown in Fig. 1b and c are the heritability values for each SBM component within the NCCC and YNPRC cohorts. For the NCCC chimpanzees, 16 of the 19 SBM components derived from the combined sample were significantly heritable. By contrast, only 8 of the 19 SBM components derived from the combined sample were significantly heritable in the YNPRC cohort. Seven of the 19 SBM components were significant in both cohorts, including components 1, 2, 4, 10, 11, and 18.

### 3.3. Combined sample: phenotypic and genetic association between tool use skill and SBM components

We initially performed partial correlation coefficients between the tool use performance data and the individual weighted scores for the 19 SBM components, while statistically controlling for relatedness, scanner, sex and age. Tool use performance was negatively associated with components 1 (*partial r* = −0.217, $p = 0.003$) and 14 (*partialr* = −0.180, $p = 0.011$) and positively associated with components 9 (*partial r* = 0.145, $p = 0.045$), 12 (*partial r* = 0.160, $p = 0.025$) and 13 (*partial r* = 0.198, $p < 0.004$). Finally, using SOLAR, we tested for genetic associations between tool use skill and components 1, 9, 12, 13 and 14. Significant genetic associations were only found between tool use skill and component 1 (*rho G* = −0.546, *se* = 0.236, $p = 0.044$), while none of the remaining components were significant.

### 3.4. SBM analyses within the NCCC and YNPRC cohorts

The SBM analyses revealed 8 and 16 components for the NCCC and YNPRC cohorts, respectively (see Supplemental Materials). Regarding phenotypic associations between tool use performance and the SBM components within the YNPRC cohort, significant negative associations were found between the performance measures and components 1 (*partial r* = −.277, $p = .026$) and 15 (*partial r* = −.251, $p = .043$) (see Fig. 2 a and b). The brain region comprising YNPRC component 1 was bilateral posterior STS region, while component 15 consisted of the middle and superior frontal gyrus (bilateral) (see Fig. 2 a and b). Within the NCCC, tool use performance was negatively associated with component 7 (*partial r* = −.213, $p = .017$) and positively associated with components 3 (*partial r* = +.224, $p = .012$) and 4 (*partial r* = +.285, $p = .001$ (see Fig. 3 a to c). Within the NCCC, brain regions comprising component 7 included bilateral STS and middle temporal gyrus. Brain regions within components 3 and 4 included inferior occipital lobe (bilateral) and lateral cerebellum (bilateral) (see Fig. 3a to c).

Of the SBM components associated with tool use performance within each cohort, component 1 within the YNPRC and component 7 within the NCCC showed considerable overlap in the brain regions comprising them (see supplementary materials). To determine the degree of similarity, we therefore performed a conjunction analysis by binarizing and thresholding components 1 (YNPRC) and 7 (NCCC) at > 3.0, then added the binary volumes together to evaluate the regions that were overlapping between these two components. As can be seen in Fig. 4, the posterior STS and superior temporal gyrus (STG) were the overlapping regions between these two components. We also performed a partial correlation coefficient between the standardized tool use performance measures within the YNPRC and NCCC colonies and the weighted scores for component 1 (YNPRC) and component 7 (NCCC) while controlling for age, sex and relatedness and found a significant negative association (*partial r* = −.193, $p = .007$). Thus, not surprising, chimpanzees that performed more poorly on the tool use task contributed less to the weighted scores for components 1 and 7, which both were comprised of the STS and STG regions.

### 3.5. Post hoc analyses of the STS

As a means of offering a more direct interpretation of the results reported here, we performed two additional post-hoc analyses. First, for the STS/STG regions defined within the conjunction analysis (see Fig. 4), we created an object map and applied it to each chimpanzee's smoothed modulated gray matter volumes on which the SBM analysis was performed. The modulated GM volume value reflect the amount of gray matter found within each voxel after application of the Jacobian warp. This generated an average amount of gray matter per voxel for the STS/STG regions for each subject. We then correlated these values with the tool use performance data for the entire sample and within each cohort. Average gray matter volume per voxel was negatively associated with tool use skill performance for the entire sample (*partial r* = −.191, $p = .007$) as well as within the NCCC (*partial r* = −.222, $p = .011$) and YNPRC (*partial r* = −.295, $p = .016$) cohorts separately.

As a follow-up to the SBM analysis, we used the software program BrainVisa to extract the STS and quantified the depth of the fold at 100 equally space locations along the anterior-posterior plane in the same sample of chimpanzees (see Fig. 5) (see Hopkins et al., 2022 for description). The more posterior regions of the STS partially overlap with the SBM regions most strongly associated with tool use skill in both cohorts (the combined C1_C7 components from the conjunction analysis). Therefore, we quantified the depth of the STS along the anterior-posterior plane and correlated these data with the tool use latency measures for the overall sample. To minimize the number of correlations, we reduced the number of fold measures along the anterior-posterior plane from 100 to 20 by averaging every 5 depth values (STS1 to STS 20). Significant negative associations were found between tool use performance and STS regions 7 to 17; thus, chimpanzees with longer latencies had more shallow STS depth measures (see Fig. 6). We also examined the phenotypic and genetic correlation between the average depth measures for STS regions 7 to 17 with the SBM component 1 weighted scores for the overall sample while controlling for scanner magnet, sex and age (see Table 3). Phenotypically, the mean STS depth for regions 7 to 17 were significantly positively correlated with the C1_C7 weighted score (*partial r* = .416, $p < .001$). Moreover, there was a significant genetic correlation (RhoG) between the mean depth of STS regions 7 to 17 with the C1_C7 SBM weighted score (*Rho G* = .684, se = .118, $p = .00007$). Indeed, there were significant phenotypic and genetic correlations between the C1_C7 weighted SBM scores and the STS depth measures for STS regions 7 to 17 (see Table 4).

## 4. Discussion

There were four main findings in the current study. First, using the updated post-image processing methods, we identified 19 gray matter SBM components in a combined sample of 216 chimpanzees. Second, all the SBM components were significantly heritable, indicating that genetic factors influence chimpanzee brain gray matter covariation. Third, for the combined sample, we found that chimpanzee performance on a tool use task designed to simulate termite fishing was associated with weighted scores of 5 SBM components. When separate SBM analyses were performed on the two chimpanzee cohorts, significant phenotypic associations were found between tool use performance and two components

within the YNPRC and three components within the NCCC cohort. The most consistent finding between the two cohorts was a negative association between tool use performance and a component that was comprised of the STS, STG, and the inferior and superior parietal cortical regions.

After refining the post-image processing methods, we identified 19 gray matter SBM components in chimpanzees. This is fewer than the 24 components previously identified using different, and simpler, post-image processing methods (Hopkins et al., 2019). Since most of the subjects participated in both studies, the difference in the number of components can likely be attributed to the post-image processing methods themselves, rather than the sample(s) per se. We not only changed the order of procedures (see Table 1 for comparison) but processed the 1.5T and 3T scans separately to account for differences in acquisition. In addition, we included both bias correction and denoising procedures that correct for illumination non-uniformity and intensity bias from Rician noise, respectively. Utilizing these correction procedures can improve the image quality, as well as subsequent segmentation, cortical surface extraction, and analyses (e.g., Acosta-Cabronero et al., 2008; Eskildsen et al., 2011; Gaser and Coupé, 2010; Sonderer and Chen, 2018). For example, none of the 18 components identified in the current study were suggestive of significant registration or segmentation artifacts (i.e., brain edges, or regions not containing gray matter), as have been reported in SBM studies of human brains (e.g., Caprihan et al., 2011; Premi et al., 2017; Xu et al., 2009) and in the previous study with chimpanzees (Hopkins et al., 2019). Therefore, it is likely that the 19 components identified in the current study are more robust, as these preprocessing steps reduced noise and illumination non-uniformity compared to the previous study. These data can now be used to more accurately examine neuroanatomical correlates of behavioral and cognitive phenotypes in these chimpanzees. For example, we have found that three of these components (7, 10, and 18 containing regions within the ventral pathway of the visual processing stream and reward circuit) are associated with mutual eye gaze behavior in chimpanzees (Hopkins et al., 2020).

Next, we found moderate to strong heritability in all 19 SBM components, indicating there are genetic factors influencing individual differences in gray matter covariation. This is supported by previous reports of genetic influences on cortical organization (e.g., surface area, sulci dimensions, gray matter volume, gyrification, etc.) in both human and nonhuman primates (Fears et al., 2009; Gomez-Robles et al., 2015; Hopkins et al., 2019; Kochunov et al., 2010; Rogers et al., 2007, 2010). When we evaluated repeatability in heritability in SBM components that were derived from either the entire sample or from separate colonies, the chimpanzees showed considerable consistency. The NCCC chimpanzees showed robust heritability in the SBM components that were derived from the combined sample or within the 8 components that were identified when their sMRI scans were processed alone. By contrast, the YNPRC chimpanzees showed less consistent heritability across components derived from both the combined and separate SBM analyses. The discrepancy in the magnitude of heritability evident between the two cohorts is potentially attributable to at least four possible factors. First, the YNPRC sample was smaller than the NCCC cohort and therefore may have had less power to detect reliable and potentially small heritability estimates in this cohort. Second, there was a larger proportion of nursery-reared compared to mother-reared chimpanzees within the YNPRC than NCCC cohort. Previous studies in

chimpanzees have shown that early rearing experiences can have a significant impact on gray matter covariation and other measures of brain organization (Bennett et al., 2021; Bogart et al., 2014). Thus, the NCCC sample consisted of chimpanzees that had a more homogenous rearing history compared to the YNPRC apes, which may have reduced the amount of error variance in the heritability statistical models. Third, differences in within colony relatedness could also be a factor; the YNPRC chimpanzees were more closely related to each other than the chimpanzees within the NCCC colony. Lastly, we cannot rule out that heritability in the chimpanzees is only moderately repeatable in the context of structural gray matter covariation when compared to findings that have focused on specific regions-of-interest when quantifying surface area or other measures of cortical structure (Gomez-Robles et al., 2015; Hopkins et al., 2015).

In addition, we found that four of the SBM components were related to tool use performance. Tool use performance was negatively correlated with two components consisting of the middle temporal cortex, inferior and superior parietal cortex, hippocampus, basal forebrain, middle and superior frontal cortex, amygdala, caudal anterior cingulate, and cerebellar cortex. Tool use performance was positively correlated with two components consisting of lingual cortex, isthmus of the cingulate, lateral occipital cortex, pericalcarine, posterior cingulate, and cerebellar cortex. In a previous study using different preprocessing methods (Hopkins et al., 2019), we found that the superior temporal sulcus, superior parietal cortex, cuneus, and primary visual cortex were phenotypically and genetically associated with tool use skill, and that these associations were all negative (those with slower latency scores contributed less to the creation of these components). These very same brain regions were identified in the current analysis and both phenotypically and genetically correlated with tool use performance. This suggests that, despite the differences in preprocessing steps, similar covarying brain regions emerged that were phenotypically and genetically associated with tool use skill.

As noted above, the most consistent brain regions related to tool use performance were the posterior STS, and inferior and superior partial cortex. These same brain regions (along with others) have been strongly implicated in the manufacture and use of tools in human subjects (Johnson-Frey, 2004; Lewis, 2006). From an evolutionary perspective, some have suggested that the function and connectivity of the inferior and superior parietal areas are unique to humans as it relates to the execution and observation of tool use actions (Cheng et al., 2021; Hecht et al., 2013; Peeters et al., 2009). Evidence of the functional role of the inferior and superior parietal regions in tool use remains unknown; however, there is at least one report showing that training macaques to use a tool resulted in increased gray matter volume in the ventral lateral and inferior parietal cortex (Quallo et al., 2009). Our findings suggest that the posterior STS, including the inferior and superior parietal cortex, played a role in tool use learning and performance in the common ancestor of humans and chimpanzees, prior to their split ~ 6 million years ago. In light of the fact that tool use is widespread among captive and wild chimpanzee populations (Shumaker et al., 2011; Whiten et al., 2001; Whiten et al., 1999), our results on heritability in tool use performance and their genetic association with gray matter covariation in the parietal cortex further suggest that there may be common genes that underlie tool using abilities in humans and chimpanzees.

There are some limitations to this study. As noted above, there are many different forms of tool use in chimpanzees. In this study, we quantified performance (latency) on a task that was designed to simulate termite fishing or ant dipping. Though this task has a significant visualmotor demand, it is unclear whether other types of tool use, particularly with different sensory and motor demands, would be associated with the parietal-frontal regions identified in this study. Additionally, as has been discussed in previous studies, it can be difficult to interpret the biological significance of SBM findings because the results do not reflect volumetric dimension of gray or white matter but rather the covariation of voxels within the components derived from independent components analysis. As a means of offering a more direct interpretation of the results reported here, we performed two additional post-hoc analyses.

First, we determined the average amount of gray matter per voxel within the STS/STG region for each subject and found that these values were negatively associated with tool use skill performance for the entire sample (and within the NCCC and YNPRC separately). Second, we quantified the depth of the STS along the anterior-posterior plane and correlated these data with the tool use latency measures for the overall sample, and found that chimpanzees with longer latencies had more shallow STS depth measures. In addition, we found that the mean STS depth for regions 7 to 17 were positively correlated with the SBM C1_C7 weighted score and that there was a significant genetic correlation (RhoG) between these two measures. In short, chimpanzees that contributed more to the creation of the C1_C7 component had deeper folds (more gyrification) in the middle and posterior regions of the STS and common genetic factors may underlie their phenotypic association.

In summary, using more refined preprocessing methods, we found 19 gray matter covariation components, 5 fewer than previously reported (Hopkins et al., 2019), but with what appears to be improved registration and less potential artifact. Consistent with previous findings, we found that tool use performance was associated with gray matter covariation in several regions but, particularly within the posterior superior temporal gyrus/sulcus and inferior and superior parietal cortex. The phenotypic association between tool use performance and gray matter covariation in the posterior STG/STS and the inferior and superior parietal cortex were consistent between two genetically independent cohorts of chimpanzees based on combined or separate SBM analysis of the sMRI scans. The findings indicate that the STG/STS and parietal cortex is phenotypically and genetically implicated in chimpanzee tool using abilities and was likely the case prior to the split from the common ancestor with humans. Future studies should focus on identifying differences and similarities in specific genes related to the motor and cognitive functions that underlie tool manufacture and use in primates, including humans.

## Supplementary Material

Refer to Web version on PubMed Central for supplementary material.

## Acknowledgements

This research was supported in part by NIH grants NS-73134, NS-42867, AG-067419, and NS-092988 (support for the National Chimpanzee Brain Resource). Chimpanzee maintenance at the National Center for Chimpanzee Care

was previously funded by NIH/NCRR U42-OD-011197. We appreciate the veterinary and caregiving staffs at both the NCCC and YNPRC for their assistance in acquiring the MRI scans.

## Data availability statement

Data are available from the National Chimpanzee Brain Resource at https://www.chimpanzeebrain.org.

## References

Acosta-Cabronero J, Williams GB, Pereira JMS, Pengas G, Nestor PJ, 2008. The impact of skull-stripping and radio-frequency bias correction on grey-matter segmentation for voxel-based morphometry. Neuroimage 39 (4), 1654–1665. doi:10.1016/j.neuroimage.2007.10.051. [PubMed: 18065243]

Almasy L, Blangero J, 1998. Multipoint quantitative-trait linkage analysis in general pedigrees. Am. J. Hum. Genet. 62, 1198–1211. [PubMed: 9545414]

Andersson JL, Jenkinson M, Smith S, 2007. Non-Linear Registration aka Spatial Normalisation. FMRIB Analysis Group of the University of Oxford FMRIB Technial Report TR07JA2.

Baker M, 2016a. 1500 scientists lift the lid on reproducibility. Nature 533 (7604), 452–454. doi:10.1038/533452a. [PubMed: 27225100]

Baker M, 2016b. Is there a reproducibilty crisis? Nature 533, 452–454. [PubMed: 27225100]

Bennett A, Pierre PJ, Wesley MJ, Latzman RD, Schapiro SJ, Mareno MC, Bradley BJ, Sherwood CC, Mulholland MM, Hopkins WD, 2021. Predicting their past: machine language learning can discriminate the brains of chimpanzees with different early-life social rearing experiences. Dev. Sci e13114. [PubMed: 34180109]

Boesch C, Boesch H, 1990. Tool use and tool making in wild chimpanzees. Folia. Primatol. 54, 86–99 (Basel).

Boesch C, Kalan AK, Agbor A, Arandjelovic M, Dieguez P, Lapeyre V, Kuhl HS, 2017. Chimpanzees routinely fish for algae with tools during the dry season in Bakoun, Guinea. Am. J. Primatol. 79 (3), 1–7. doi:10.1002/ajp.22613.

Bogart SL, Bennett AJ, Schapiro SJ, Reamer LA, Hopkins WD, 2014. Different early rearing experiences have long-term effects on cortical organization in captive chimpanzees (Pan Troglodytes). Dev. Sci. 17 (2), 161–174. doi:10.1111/desc.12106. [PubMed: 24206013]

Boyes RG, Gunter JL, Frost C, Janke AL, Yeatman T, Hill DL, Bernstein MA, Thompson PM, Weiner MW, Schuff N, 2008. Intensity non-uniformity correction using N3 on 3-T scanners with multichannel phased array coils. Neuroimage 39 (4), 1752–1762. https://www.ncbi.nlm.nih.gov/pmc/articles/PMC2562663/pdf/nihms-48435.pdf. [PubMed: 18063391]

Boysen ST, Kuhlmeier K, Halliday P, Halliday YM, 1999. Tool use in captive gorillas. In: Parker ST, Mitchell RW, Miles HL (Eds.), The Mentality of Gorillas and Orangutans. Cambridge University Press.

Bradshaw JL, Rogers LJ, 1993. The Evolution of Lateral Asymmetries, Language, Tool Use, and Intellect. Academic Press, Inc.

Candland D, 1987. Tool use. In: Mitchell G, Erwin JM (Eds.), Comparative Primate Biology; Vol 2, Part B: Behavior, Cognition and Motivation. Alan R. Liss, pp. 85–103.

Caprihan A, Abbott C, Yamamoto J, Pearlson G, Permone-Bizzozero N, Sui J, Calhoun VD, 2011. Source-based morphometry analysis of group differences in fractional anisotropy in Schizophrenia. Brain Connectiv. 1 (2), 133–145.

Cheng L, Zhang Y, Li G, Wang J, Sherwood C, Gong G, Fan L, Jiang T, 2021. Connectional asymmetry of the inferior parietal lobule shapes hemispheric specialization in humans, chimpanzees, and rhesus macaques. Elife 10. doi:10.7554/eLife.67600.

Coupé P, Yger P, Prima S, Hellier P, Kervrann C, Barillot C, 2008. An optimized blockwise nonlocal means denoising filter for 3-D magnetic resonance images. IEEE Trans. Med. Imaging 27 (4), 425–441. [PubMed: 18390341]

Douaud G, Smith S, Jenkinson M, Behrens T, Johansen-Berg H, Vickers J, James S, Voets N, Watkins K, Matthews PM, 2007. Anatomically related grey and white matter abnormalities in adolescent-onset schizophrenia. Brain 130 (9), 2375–2386. [PubMed: 17698497]

Eskildsen S, Coupé P, Fonov V, Ostergaard LR, Collins L (2011). Impact of non-local means filtering on brain tissue segmentation. In Organization for Human Brain Mapping 2010 Annual Meeting.

Fears SC, Melega WP, Service SK, Lee C, Chen K, Tu Z, Jorgensen MJ, Fairbanks LA, Cantor RM, Freimer NB, Woods RP, 2009. Identifying heritable brain phenotypes in an extended pedigree of vervet monkeys. J. Neurosci. 29 (9), 2867–2875. [PubMed: 19261882]

Fedorov A, Beichel R, Kalpathy-Cramer J, Finet J, Fillion-Robin JC, Pujol S, Bauer C, Jennings D, Fennessy F, Sonka M, Buatti J, Aylward S, Miller JV, Pieper S, Kikinis R, 2012. 3D slicer as an image computing platform for the quantitative imaging network. Magn. Reson. Imaging 30 (9), 1323–1341. doi:10.1016/j.mri.2012.05.001. [PubMed: 22770690]

Fragaszy D, Izar P, Visalberghi E, Ottoni EB, Oliveira MG, 2004. Wild capuchin monkeys (Cebus libidinosus) use anvils and stone pounding tools. Am. J. Primatol. 64, 359–366. [PubMed: 15580579]

Gaser C, Coupé P, 2010, June. Impact of non-local means filtering on brain tissue segmentation. In Organization for Human Brain Mapping 2010 Annual Meeting.

Gibson KR, Ingold T, 1993. Tools, Language and Cognition in Human Evolution. Tools, Language and Cognition in Human Evolution. Cambridge University Press.

Gomez-Robles A, Hopkins WD, Schapiro SJ, Sherwood CC, 2015. Relaxed genetic control of cortical organization in human brains compared with chimpanzees. Proc. Natl. Acad. Sci. U. S. A. 112 (48), 14799–14804. doi:10.1073/pnas. 12. [PubMed: 26627234]

Gupta CN, Turner JA, Calhoun VD, 2019. Source-based morphometry: a decade of covarying structural brain patterns. Brain Struct. Funct. 224 (9), 3031–3044. [PubMed: 31701266]

Hara Y, Rapp PR, Morrison JH, 2012. Neuronal and morphological bases of cognitive decline in aged rhesus monkeys. Age 34 (5), 1051–1073. [PubMed: 21710198]

Hecht EE, M LE, Gutman DA, Votaw JR, Schuster DM, Preuss TM, Orban GA, Stout D, Parr LA, 2013. Differences in neural activation for object-directed grasping in chimpanzees and humans. J. Neurosci. 33 (35), 14117–14134. [PubMed: 23986247]

Hopkins WD, Avants BB, 2013. Regional and hemispheric variation in cortical thickness in chimpanzees (Pan Troglodytes). J. Neurosci. 33, 5241–5248. [PubMed: 23516289]

Hopkins WD, Coulon O, Meguerditchian A, Staes N, Sherwood CC, Schapiro SJ, Mangin JF, Bradley BA, 2022. Genetic determinants of individual variation in the superior temporal sulcus of chimpanzees (Pan Troglodytes). Cereb. Cortex.

Hopkins WD, Latzman RD, Mareno MC, Schapiro SJ, Gómez-Robles A, Sherwood CC, 2019. Heritability of gray matter structural covariation and tool use skills in chimpanzees (Pan Troglodytes): a source-based morphometry and quantitative genetic analysis. Cereb. Cortex 29 (9), 3702–3711. doi:10.1093/cercor/bhy250. [PubMed: 30307488]

Hopkins WD, Mareno MC, Schapiro SJ, 2019. Further evidence of left hemisphere dominance in motor skill by chimpanzees on a tool use task. J. Comp. Psychol. 133 (4), 512–519. [PubMed: 31246047]

Hopkins WD, Misiura M, Pope SM, Latash EM, 2015. Behavioral and brain asymmetries in primates: a preliminary evaluation of two evolutionary hypotheses. Yearb. Cogn. Neurosci. 1359, 65–83.

Hopkins WD, Mulholland MM, Reamer LA, Mareno MC, Schapiro SJ, 2020. The role of early social rearing, neurological and genetic factors on individual differences in mutual eye gaze among captive chimpanzees. Sci. Rep. 10, 1–10. doi:10.1038/s41598-020-64051-y. [PubMed: 31913322]

Hopkins WD, Reamer L, Mareno MC, Schapiro SJ, 2015. Genetic basis for motor skill and hand preference for tool use in chimpanzees (Pan Troglodytes). Proc. R. Soc. Biol. Sci. B 282 (1800).

Hopkins WD, Westerhausen R, Schapiro S, Sherwood CC, 2022. Heritability in corpus callosum morphology and its association with tool use skill in chimpanzees (Pan Troglodytes): reproducibility in two genetically isolated populations. Genes Brain Behav. e12784. doi:10.1111/gbb.12784. [PubMed: 35044083]

Jenkinson M, Bannister P, Brady M, Smith S, 2002. Improved optimization for the robust and accurate linear registration and motion correction of brain images. Neuroimage 17 (2), 825–841. [PubMed: 12377157]

Jenkinson M, Pechaud M, Smith S, 2005. BET2: MR-based estimation of brain, skull and scalp surfaces. In: Proceedings of the 11th Annual Meeting of the Organization for Human Brain Mapping, 17, p. 167.

Jenkinson M, Smith S, 2001. A global optimisation method for robust affine registration of brain images. Med. Image Anal. 5 (2), 143–156. [PubMed: 11516708]

Johnson-Frey SH, 2004. The neural basis of complex tool use in humans. Trends Cogn. Sci. 8 (2), 71–78. [PubMed: 15588811]

Kikinis R, Pieper SD, Vosburgh KG, 2014. 3D Slicer: a platform for subject-specific image analysis, visualization, and clinical support. In: Intraoperative Imaging and Image-Guided Therapy. Springer, pp. 277–289.

Kochunov PV, Glahn DC, Fox PT, Lancaster JL, Saleem KS, Shelledy W, Zilles K, Thompson PM, Coulon O, Mangin JF, Blangero J, Rogers J, 2010. Genetics of primary cerebral gyrification: heritability of length, depth and area of primary sulci in an extended pedigree of Papio baboons. Neuroimage 53 (3), 1126–1134. [PubMed: 20035879]

Lazic SE, 2010. The problem of pseudoreplication in neuroscientific studies: it is affecting your analysis? BMC: Neurosci. 11, 5. [PubMed: 20074371]

Lewis JW, 2006. Cortical networks related to human use of tools. Neuroscientist 12 (3), 211–231. [PubMed: 16684967]

McArthur SL, 2019. Repeatability, reproducibility, and replicability: tackling the 3R challenge in biointerface science and engineering. Biointerphases 14 (2), 020201. doi:10.1116/1.5093621. [PubMed: 30845806]

Mendes N, Hanus D, Call J, 2007. Raising the level: orangutans use water as a tool. Biol. Lett. 3, 453–455. [PubMed: 17609175]

Moura DAAC, Lee PC, 2004. Capuchin stone tool use in Caatinga dry forest. Science 306 (10), 1909. [PubMed: 15591195]

Mulholland MM, Navabpour SV, Mareno MC, Schapiro SJ, Young LJ, Hopkins WD, 2020. AVPR1A variation is linked to gray matter covariation in the social brain network of chimpanzees. Genes Brain Behav. 19, e12631. doi:10.1111/gbb.12631. [PubMed: 31894656]

Peeters R, Simone L, Nelissen K, Orban GA, 2009. The representation of tool use in humans and monkeys: common and uniquely human features. J. Neurosci. 29 (37), 11523–11539. [PubMed: 19759300]

Phillips KA, 1998. Tool use in wild capuchin monkeys (Cebus albifrons trinitatis). Am. J. Primatol. 46, 259–261. [PubMed: 9802515]

Premi E, Calhoun VD, Garibotto V, Turrone R, Alberici A, Cottini E, Pilotto A, Gazzina S, Magoni M, Paghera B, Borroni B, Padovani A, 2017. Source-based morphometry multivariate approach to analyze [123I]FP-CIT SPECT imaging. Mol. Imaging Biol. 19 (5), 772–778. doi:10.1007/s11307-017-1052-3. [PubMed: 28194630]

Pruetz JD, Bertolani P, 2007. Savanna chimpanzees (Pan trogodytes verus) hunt with tools. Curr. Biol. 17 (5), 412–417. [PubMed: 17320393]

Quallo MM, Price CJ, Ueno K, Asamizuya T, Cheng K, Lemon RN, Iriki A, 2009. Gray and white matter changes associated with tool-use learning in macaque monkeys. Proc. Natl. Acad. Sci. 106 (43), 18379–18384. [PubMed: 19820167]

Rogers J, Kochunov PV, Lancaster JL, Sheeledy W, Glahn D, Blangero J, Fox PT, 2007. Heritability of brain volume, surface area and shape: an MRI study in an extended pedigree of baboons. Hum. Brain Mapp. 28, 576–583. [PubMed: 17437285]

Rogers J, Kochunov PV, Zilles K, Shelledy W, Lancaster JL, Thompson P, Duggirala R, Blangero J, Fox PT, Glahn DC, 2010. On the genetic architecture of cortical folding and brain volume in primates. Neuroimage 53, 1103–1108. [PubMed: 20176115]

Sanz CM, Morgan DB, 2007. Chimpanzee tool technology in the goualougo triangle, republic of Congo. J. Hum. Evol. 52 (4), 420–433. doi:10.1016/j.jhevol.2006.11.001. [PubMed: 17194468]

Shumaker RW, Wallup KR, Beck BB, 2011. Animal Tool Behavior: The Use and Manufacture of Tools by Animals. Johns Hopkins University Press.

Smith SM, 2002. Fast robust automated brain extraction. Hum. Brain Mapp. 17 (3), 143–155. doi:10.1002/hbm.10062. [PubMed: 12391568]

Smith SM, Jenkinson M, Woolrich MW, Beckmann CF, Behrens TE, Johansen-Berg H, Bannister PR, De Luca M, Drobnjak I, Flitney DE, 2004. Advances in functional and structural MR image analysis and implementation as FSL. Neuroimage 23, S208–S219. [PubMed: 15501092]

Sonderer CM, Chen N, 2018. Improving the accuracy, quality, and signal-to-noise ratio of MRI parametric mapping using rician bias correction and parametric-contrast–matched principal component analysis (PCM-PCA). Yale J. Biol. Med. 91 (3), 207–214. [PubMed: 30258307]

Tustison N, Avants BB, Cook PA, Gee JC, 2010. N4itk: Improved n3 bias correction with robust b-spline approximation. In: Proceedings of the ISBI.

Tustison N, Gee J, 2009. N4ITK: nick's N3 ITK implementation for MRI bias field correction. Insight J 9.

Tustison NJ, Avants BB, Cook PA, Zheng Y, Egan A, Yushkevich PA, Gee JC, 2010. N4ITK: improved N3 bias correction. IEEE Trans. Med. Imaging 29 (6), 1310–1320. doi:10.1109/TMI.2010.2046908. [PubMed: 20378467]

Tustison NJ, Cook PA, Klein A, Song G, Das SR, Duda JT, Kandel BM, van Strien N, Stone JR, Gee JC, Avants BB, 2014. Large-scale evaluation of ANTs and FreeSurfer cortical thickness measurements. Neuroimage 99, 166–179. doi:10.1016/j.neuroimage.2014.05.044. [PubMed: 24879923]

Vaesen K, 2012. The cognitive bases of human tool use. Behav. Brain Sci. 35, 203–262. [PubMed: 22697258]

Van Schaik CP, Ancrenaz M, Borgen G, Galdikas B, Knott CD, Singleton I, Suzuki A, Utami SS, Merrill M, 2003. Orangutan culture and the evolution of material culture. Science 299 (102–205).

Van Schaik CP, Deaner RO, Merrill MY, 1999. The conditions for tool use in primates: implications for the evolution of material culture. J. Hum. Evol. 36, 719–741. [PubMed: 10330335]

Visalberghi E, 1990. Tool use in Cebus. Folia. Primatol. 54, 146–154 (Basel).

Whiten A, Goodall J, McGrew W, Nishida T, Reynolds V, Sugiyama Y, Tutin C, Wrangham R, Boesch C, 2001. Charting cultural variation in chimpanzees. Behaviour 138, 1489–1525.

Whiten A, Goodall J, McGrew WC, Nishida T, Reynolds V, Sugiyama Y, Tutin CEG, Wrangham RW, Boesch C, 1999. Cultures in chimpanzees. Nature 399, 682–685. [PubMed: 10385119]

Xu L, Groth KM, Pearlson G, Schreffen DJ, Calhoun VD, 2009. Source-based morphometry: the use of independent component analysis to identify gray matter differences with application to schizophrenia. Hum. Brain Mapp. 30 (3), 711–724. [PubMed: 18266214]

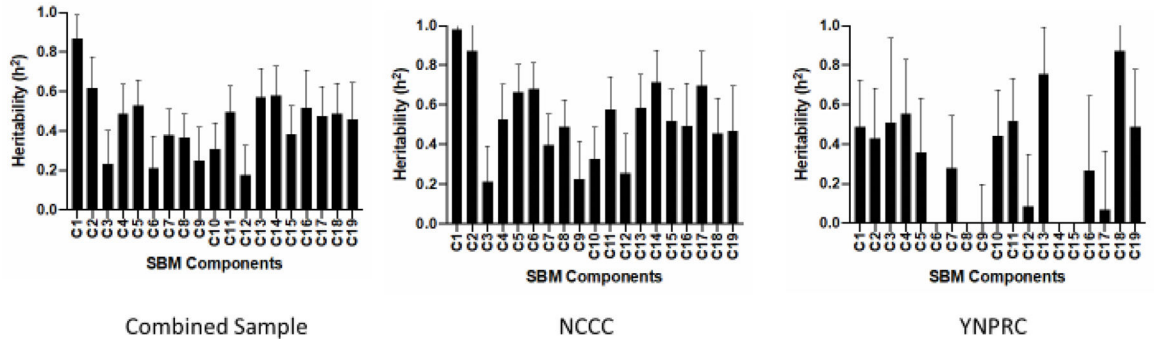


**Fig. 1.**

Heritability (+/− s.e.) values for the 19 SBM components for the combined, NCCC and YNPRC cohorts.

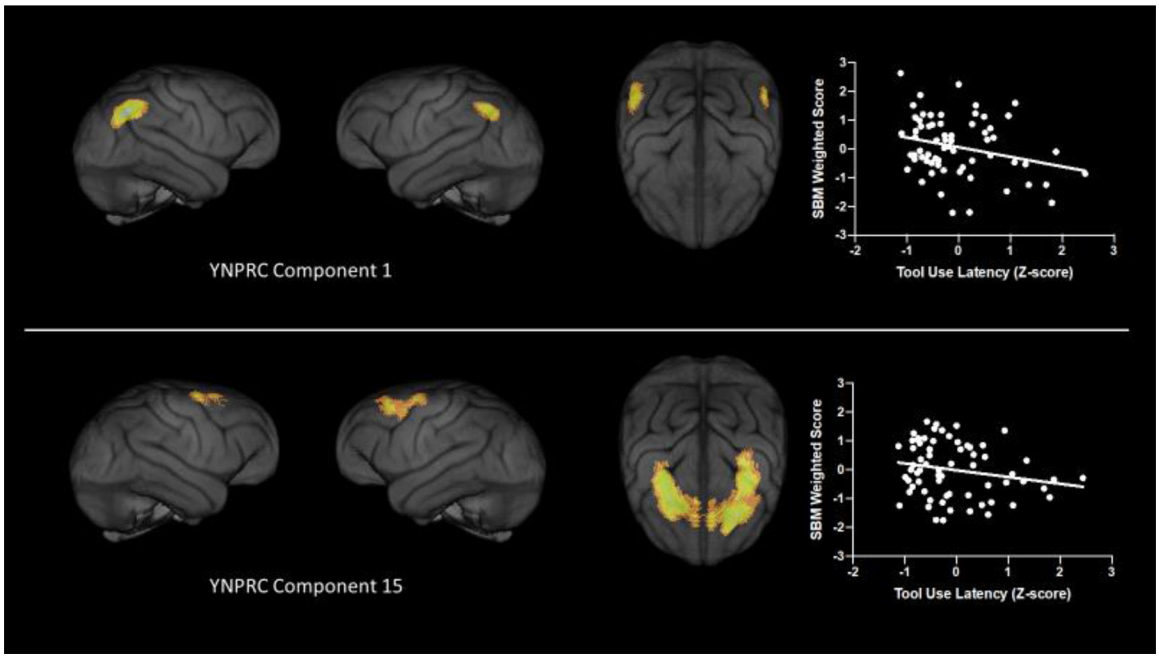


**Fig. 2.**

3-D lateral and superior renderings of gray matter covariation brain regions in components 1 (upper panel) and 15 (lower panel) that were associated with tool use performance in the YNPRC cohort. Far right image within each panel shows scatterplot of the association between tool use performance and the weighted component scores.

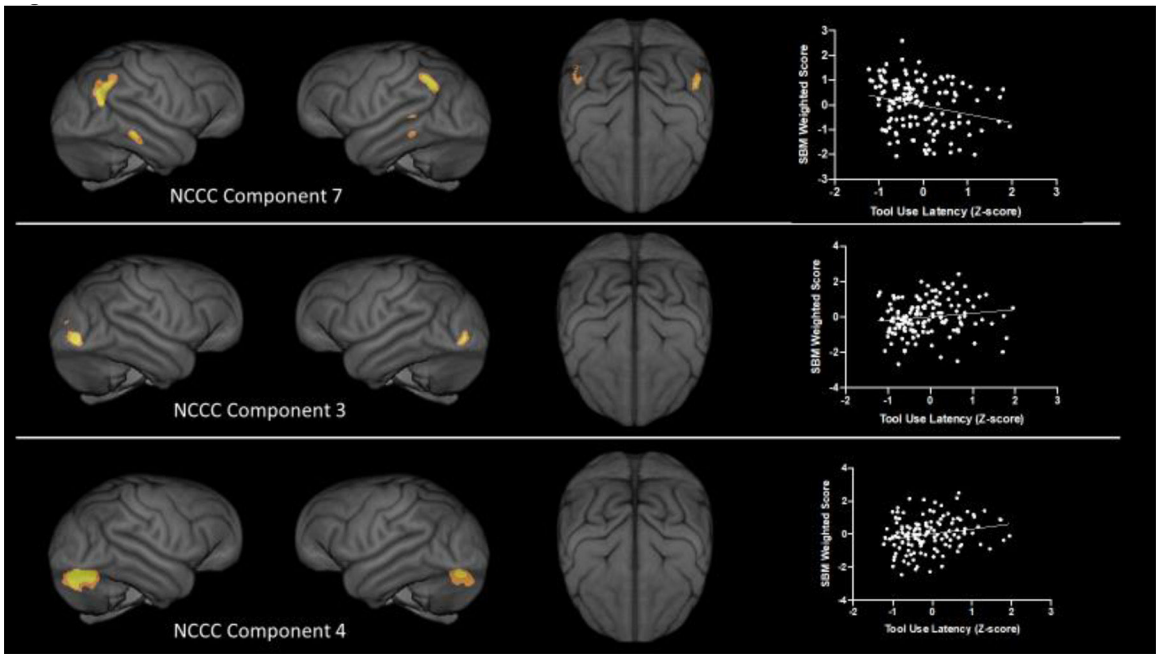


**Fig. 3.**

3-D lateral and superior renderings of gray matter covariation brain regions in components 7 (upper panel), 12 (middle panel) and 13 (lower panel) that were associated with tool use performance in the NCCC cohort. Far right image within each panel shows scatterplot of the association between tool use performance and the weighted component scores.

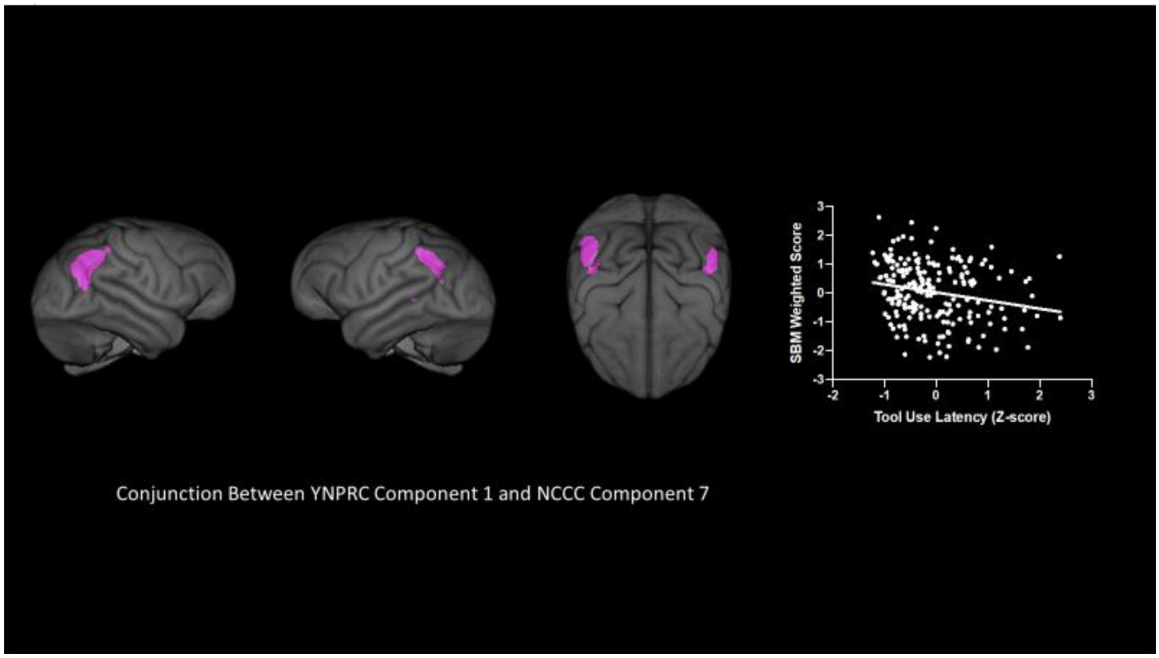


**Fig. 4.**

3-D rendering of regions that were overlapping between YPRC Component 1 and NCCC Component 7 in the conjunction analysis. Far right image shows scatterplot of the association between tool use performance and the weighted component scores.

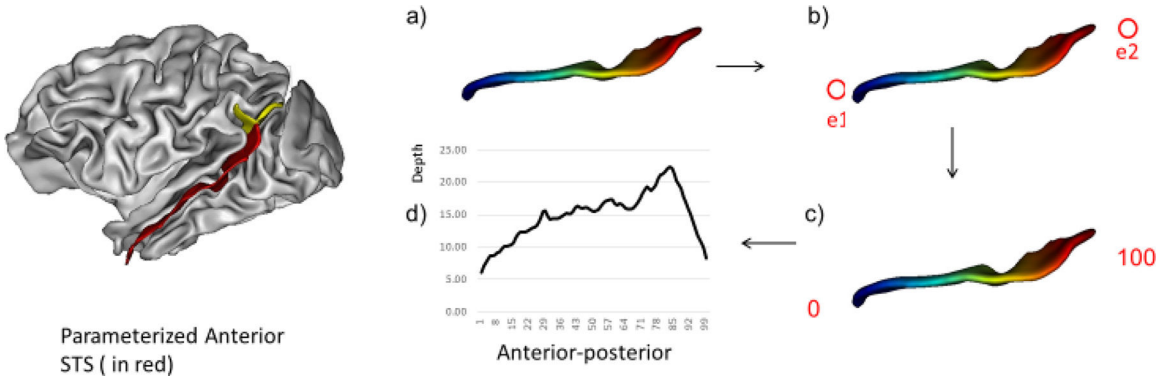


**Fig. 5.**

(Left panel) 3-D rendering of chimpanzee brain using BrainVisa with the STS labeled. In red, is the main section of the STS that was parameterized for these analyses. The portion of the posterior STS that bifurcated (in yellow) was excluded from the parametrization analysis. (Right panel)

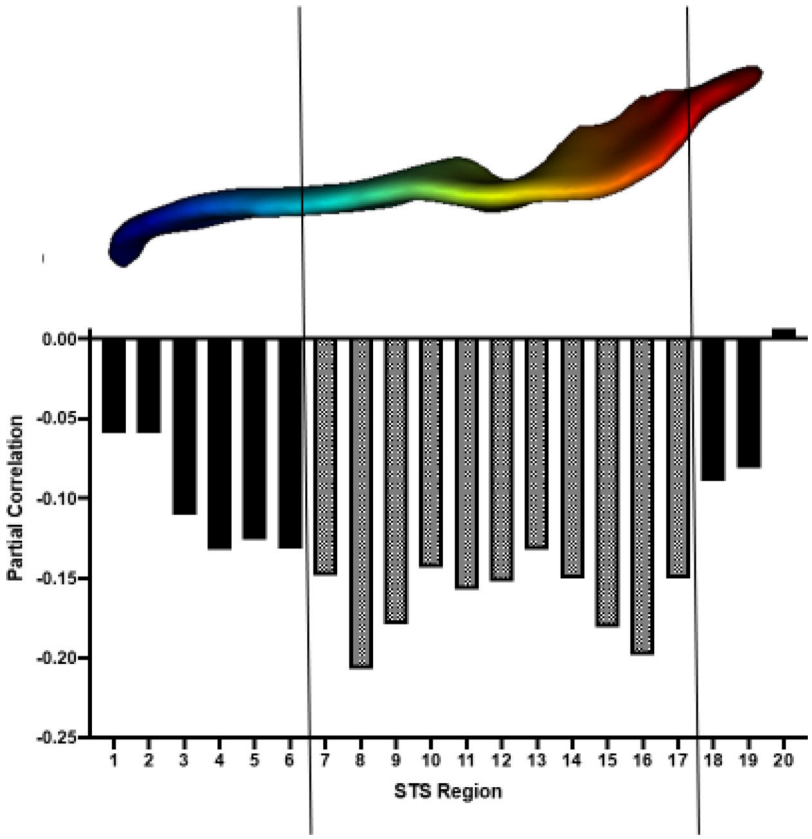


**Fig. 6.**

Upper panel is display of extracted STS. Lower panel shows the partial correlation coefficients between tool use performance and the depth of the STS fold in the 20 STS regions. Dashed regions are significant at $p < .05$.

**Table 1**

Comparison of post-image processing methods between the current and previous study (Hopkins et al., 2019) of gray matter covariation in chimpanzees.

| **Current Study** | **Hopkins et al. (2019) Study** |
|---|---|
| 1. Skull stripping (BET function; FSL) | 1. AC-PC alignment |
| 2. N4ITK bias correction (3D SLicer) | 2. Skull Stripping (BET function; FSL) |
| 3. ONLM denoising (MRI denoising; Matlab) | 3. Resampling at .7 mm isotropic voxels |
| 4. Resampling at .625 mm isotropic voxels and AC-PC alignment (Analyze 11.0) | 4. FSL-VBM pipeline |
| | a. segmentation |
| 5. 12 parameter affine linear registration to template brain (FLIRT function; FSL) | b. linear registration to a standard chimpanzee template |
| | c. creation of a study-specific template |
| 6. FSL-VBM pipeline (separate for 1.5T & 3T scans) | d. nonlinear registration of individual gray matter volumes to the study-specific template |
| a. segmentation | |
| b. linear registration to a standard chimpanzee template | e. modulation of gray matter volumes |
| c. creation of a study-specific template | f. smoothing |
| d. nonlinear registration of individual gray matter volumes to the study-specific template | |
| e. modulation of gray matter volumes | |
| f. smoothing | |
| 7. 6 parameter rigid-body linear registration to template brain (FLIRT function; FSL) | |

**Table 2**

Regions and corresponding volumes ($mm^3$; ≥ 40) of the 19 SBM components.

| Region | Total volume | L/R volume |
|---|---|---|
| **Component 1** | | |
| Supramarginal | 7586.42 | 4351.56 / 3234.86 |
| bankssts | 960.70 | 361.33 / 599.37 |
| superior parietal cortex | 382.32 | 168.21 / 214.11 |
| precuneus | 359.86 | 109.62 / 250.24 |
| inferior temporal cortex | 164.07 | 15.14 / 148.93 |
| cerebellar cortex (CerIV, CerIX) | 75.44 | 0 / 75.44 |
| **Component 2** | | |
| middle & superior temporal cortex (incl. bankssts) | 7160.16 | 2828.37 / 4331.79 |
| lateral occipital cortex | 510.99 | 510.99 / 0 |
| superior parietal cortex | 421.63 | 114.75 / 306.88 |
| precuneus | 363.03 | 191.89 / 171.14 |
| fusiform | 263.92 | 140.38 / 123.54 |
| caudal middle frontal cortex | 232.91 | 232.91 / 0 |
| precentral gyrus | 191.89 | 414.79 / 123.54 |
| insular cortex | 191.89 | 63.23 / 128.66 |
| supramarginal | 63.23 | 63.23 / 0 |
| inferior parietal cortex | 52.49 | 52.49 / 0 |
| **Component 3** | | |
| temporal pole, amygdala, & fusiform gyrus | 9864.74 | 4862.79 / 5001.95 |
| **Component 4** | | |
| cerebellar cortex (CerVB, CerVI, CrusI, CrusII) | 8110.84 | 4640.87 / 3469.97 |
| lateral occipital cortex | 1435.55 | 948.00 / 487.55 |
| superior parietal cortex | 119.38 | 119.38 / 0 |
| rostral middle frontal cortex | 89.36 | 89.36 / 0 |
| **Component 5** | | |
| superior parietal cortex | 8110.84 | 2200.44 / 1982.67 |
| posterior cingulate & paracentral gyrus | 1281.25 | 702.64 / 578.61 |

| Region | Total volume | L/R volume |
|---|---|---|
| postcentral gyrus | 1036.38 | 485.35 / 551.03 |
| precentral gyrus | 456.06 | 202.15 / 253.91 |
| superior temporal cortex & bankssts | 415.28 | 415.28 / 0 |
| superior parietal cortex | 406.25 | 270.26 / 135.99 |
| pars opercularis | 375.97 | 23.19 / 352.78 |
| superior frontal cortex | 350.34 | 273.44 / 76.90 |
| precuneus | 262.21 | 111.82 / 150.39 |
| insular cortex | 225.59 | 225.59 / 0 |
| medial orbital frontal cortex | 137.45 | 53.47 / 83.98 |
| inferior parietal cortex | 95.95 | 70.31 / 25.64 |
| caudal middle frontal cortex | 64.21 | 64.21 / 0 |
| precentral gyrus | 61.04 | 0 / 61.04 |
| rostral middle frontal cortex | 56.15 | 0 / 56.15 |
| entorhinal cortex | 53.95 | 35.64 / 18.31 |
| **Component 6** | | |
| precuneus & superior parietal cortex | 3633.30 | 1721.92 / 1911.38 |
| frontal pole | 3272.71 | 1563.48 / 1709.23 |
| precuneus | 2973.15 | 1331.79 / 1641.36 |
| caudal and rostral middle frontal cortex | 707.77 | 346.93 / 360.84 |
| lingual cortex | 152.10 | 62.74 / 89.36 |
| medial orbital frontal cortex | 73.00 | 73.00 / 0 |
| precentral gyrus | 59.57 | 59.57 / 0 |
| **Component 7** | | |
| rostral middle frontal cortex, superior frontal cortex, & pars triangularis | 6174.32 | 4160.16 / 2014.16 |
| superior parietal cortex | 1486.82 | 786.87 / 699.95 |
| caudal middle frontal cortex | 805.18 | 805.18 / 0 |
| posterior & caudal anterior cingulate cortex & paracentral | 516.60 | 0 / 516.60 |
| cerebellar cortex (CerVI, CrusII) | 493.16 | 0/ 493.16 |
| postcentral gyrus | 435.05 | 79.83 / 355.22 |
| posterior cingulate | 367.92 | 367.92 / 0 |
| inferior parietal cortex | 344.24 | 10.99 / 333.25 |

| Region | Total volume | L/R volume |
|---|---|---|
| lingual cortex | 124.03 | 47.61 / 76.42 |
| precentral gyrus | 123.04 | 73.97 / 49.07 |
| superior parietal cortex & paracentral | 94.73 | 0 / 94.73 |
| **Component 8** | | |
| superior parietal cortex, precuneus, paracentral, postcentral and precentral gyri | 11784.18 | 5947.75 / 5836.43 |
| **Component 9** | | |
| lingual cortex, pericalcarine, cuneus | 6150.63 | 3321.04 / 2829.59 |
| cerebellar cortex (CerVA, CerVB, CerIX, CrusII) | 3376.46 | 1295.41 / 2081.05 |
| superior parietal & precuneus | 619.87 | 374.02 / 245.85 |
| cerebellar cortex (CerVI, CrusI) | 70.07 | 70.07 / 0 |
| **Component 10** | | |
| medial orbital frontal cortex, rostral anterior cingulate cortex, & accumbens area | 5431.88 | 2814.45 / 2617.43 |
| lateral orbital frontal cortex, insular cortex, & pars opercularis | 1466.30 | 906.49 / 559.81 |
| superior frontal cortex | 781.25 | 356.93 / 424.32 |
| precuneus | 105.47 | 14.16 / 91.31 |
| caudal middle frontal cortex | 88.87 | 88.87 / 0 |
| **Component 11** | | |
| rostral middle & caudal middle frontal cortex, & precentral gyrus | 9409.92 | 4637.21 / 4772.71 |
| superior frontal cortex & caudal anterior cingulate cortex | 3382.57 | 1651.61 / 1730.96 |
| insular cortex | 111.32 | 102.78 / 8.54 |
| **Component 12** | | |
| cerebellar cortex (CerIV, CerVA, CerVB, CerVI, CerVIII, CerIX) | 7199.95 | 3695.31 / 3504.64 |
| lingual cortex & isthmus cingulate | 5504.64 | 3142.58 / 2362.06 |
| precuneus | 322.75 | 140.62 / 182.13 |
| lateral occipital cortex | 101.81 | 0 / 101.81 |
| **Component 13** | | |
| lateral occipital cortex & inferior parietal | 9972.17 | 4826.42 / 5145.75 |
| pericalcarine & fusiform gyrus | 834.96 | 406.49 / 428.47 |
| cerebellar cortex (CerVI) | 806.89 | 590.09 / 216.80 |
| supramarginal | 184.08 | 161.13 / 22.95 |
| isthmus cingulate, posterior cingulate, & precuneus | 91.07 | 50.54 / 40.53 |

| Region | Total volume | L/R volume |
|---|---|---|
| **Component 14** | | |
| (anterior) superior, middle, & inferior temporal cortex, temporal pole, & hippocampus | 6358.40 | 4123.29 / 2235.11 |
| cerebellar cortex (CerII, CerIII, CerIV, CerVA, CerVB, CerVI) | 5532.96 | 2832.76 / 2700.20 |
| accumbens area, caudate, & putamen | 3189.94 | 1438.23 / 1751.71 |
| rostral middle & superior frontal cortex | 1501.46 | 384.03 / 1117.43 |
| lingual cortex & fusiform gyrus | 1000.73 | 460.45 / 540.28 |
| entorhinal cortex & amygdala | 959.72 | 528.81 / 430.91 |
| caudal anterior cingulate cortex & superior frontal cortex | 489.75 | 236.33 / 253.42 |
| superior parietal & precuneus | 468.75 | 238.04 / 230.71 |
| pars triangularis & pars opercularis | 377.93 | 0 / 377.93 |
| amygdala | 374.75 | 163.57 / 211.18 |
| inferior parietal cortex | 256.84 | 256.84 / 0 |
| paracentral | 219.97 | 104.98 / 114.99 |
| precentral gyrus | 148.19 | 148.19 / 0 |
| bankssts | 93.02 | 0 / 93.02 |
| superior parietal cortex | 57.37 | 0 / 57.37 |
| **Component 15** | | |
| cerebellar cortex (Cer VIII, CerIX, Crus II) | 1622.80 | 735.35 / 887.45 |
| inferior parietal cortex | 127.94 | 109.62 / 18.32 |
| **Component 16** | | |
| cerebellar cortex (CerVI, CerVIII, CerIX, CrusI, CrusII) | 13240.48 | 6747.56 / 6492.92 |
| **Component 17** | | |
| precuneus, inferior parietal cortex & lateral occipital cortex | 10061.53 | 4881.35 / 5180.18 |
| superior parietal cortex | 1249.75 | 579.10 / 670.65 |
| posterior cingulate & precuneus | 308.59 | 150.63 / 157.96 |
| lateral occipital cortex | 87.89 | 47.85 / 40.04 |
| **Component 18** | | |
| accumbens area, caudate, putamen, & pallidum | 3169.19 | 1443.12 / 1726.07 |
| hippocampus | 1770.26 | 858.15 / 912.11 |
| medial orbital frontal cortex | 1470.22 | 865.97 / 604.25 |
| caudal middle frontal cortex & pars opercularis | 1167.96 | 496.09 / 671.87 |

| Region | Total volume | L/R volume |
|---|---|---|
| superior frontal cortex | 460.69 | 18.31 / 442.38 |
| caudal anterior cingulate cortex | 438.23 | 187.74 / 250.49 |
| precentral gyrus | 310.79 | 310.79 / 0 |
| rostral middle frontal cortex | 159.67 | 74.46 / 85.21 |
| lateral occipital cortex | 100.34 | 100.34 / 0 |
| (anterior) superior temporal cortex | 58.11 | 0 / 58.11 |
| inferior parietal cortex | 42.24 | 42.24 / 0 |
| **Component 19** | | |
| superior frontal cortex, rostral anterior & caudal anterior cingulate cortex | 9702.64 | 5193.12 / 4509.52 |
| posterior cingulate & paracentral | 354.01 | 159.67 / 194.34 |
| cerebellar cortex (CrusII) | 219.73 | 0 / 219.73 |
| caudal middle frontal cortex | 193.85 | 15.87 / 177.98 |
| precuneus | 112.06 | 45.41 / 66.65 |
| pars triangularis | 92.53 | 39.06 / 53.47 |

**Table 3.**

The heritability value ($h^2$) ± standard error (p-value) for the combined 19 source-based morphometry components.

| Component | $h^2$ ± se | p | Covariates | Variance Explained |
|---|---|---|---|---|
| **1** | **0.868 ± 0.118** | **0.000000001** | All | 0.254 |
| **2** | **0.615 ± 0.159** | **0.00003** | Scanner, Age | 0.323 |
| 3 | 0.231 ± 0.171 | 0.072 | Scanner, Age | 0.189 |
| **4** | **0.486 ± 0.152** | **0.0003** | All | 0.206 |
| **5** | **0.529 ± 0.127** | **0.000007** | Sex | 0.029 |
| 6 | 0.212 ± 0.162 | 0.081 | Sex, Age | 0.056 |
| **7** | **0.379 ± 0.133** | **0.0004** | None | 0.000 |
| **8** | **0.364 ± 0.121** | **0.0001** | Scanner, Age | 0.432 |
| 9 | 0.249 ± 0.169 | 0.054 | Sex, Scanner | 0.463 |
| **10** | **0.307 ± 0.133** | **0.005** | Scanner, Age | 0.339 |
| **11** | **0.495 ± 0.134** | **0.00006** | Scanner, Age | 0.354 |
| 12 | 0.177 ± 0.151 | 0.1 | Scanner | 0.256 |
| **13** | **0.571 ± 0.144** | **0.000008** | All | 0.348 |
| **14** | **0.578 ± 0.152** | **0.0001** | Scanner, Age | 0.483 |
| **15** | **0.384 ± 0.143** | **0.001** | Scanner, Age | 0.454 |
| **16** | **0.516 ± 0.189** | **0.003** | Scanner | 0.432 |
| **17** | **0.473 ± 0.149** | **0.0004** | Scanner, Sex | 0.291 |
| **18** | **0.488 ± 0.152** | **0.0005** | Scanner | 0.439 |
| **19** | **0.458 ± 0.186** | **0.004** | Scanner, Age | 0.045 |

Significant heritability values at the $p < 0.05$ level are indicated with bold text. Significant covariates at the $p < 0.10$ level are listed, along with the proportion of the variance explained by the covariates [*Note*: All indicates that all three covariates, including sex, age, and scanner, were significant].

**Table 4:**

Phenotypic and genetic correlations between the STS depth measures and the combined SBM C1_C7 weighted scores.

| $H^2$ | Phenotypic | RhoG | se | p |
|---|---|---|---|---|
| STS1 | −0.029 | | | |
| STS2 | +0.045 | | | |
| STS3 | +0.100 | −.129 | .369 | .7156 |
| STS4 | +0.119 | .164 | .285 | .5903 |
| STS5 | +0.109 | .273 | .254 | .3313 |
| STS6 | +0.117 | .308 | .194 | .1578 |
| **STS7** | **+0.156** | **.389** | **.165** | **.0447** |
| **STS8** | **+0.239** | **.524** | **.145** | **.0053** |
| **STS9** | **+0.268** | **.558** | **.147** | **.0035** |
| **STS10** | **+0.298** | **.575** | **.144** | **.0025** |
| **STS11** | **+0.356** | **.643** | **.131** | **.0005** |
| **STS12** | **+0.389** | **.700** | **.134** | **.0005** |
| **STS13** | **+0.387** | **.678** | **.128** | **.0002** |
| **STS14** | **+0.413** | **.625** | **.127** | **.0001** |
| **STS15** | **+0.398** | **.655** | **.147** | **.0003** |
| **STS16** | **+0.409** | **.783** | **.178** | **.0002** |
| **STS17** | **+0.434** | **.783** | **.146** | **.00006** |
| **STS18** | **+0.342** | **.725** | **.273** | **.002** |
| STS19 | +0.277 | | | |
| STS20 | +0.171 | .867 | .838 | .0662 |
| **STS7to17** | **+0.416** | **.684** | **.118** | **.00007** |

Significant correlations are indicated with bold text.